Michigan State University

National Superconducting Cyclotron Laboratory

DYNAMICAL EFFECTS IN FUSION REACTIONS FORMING ^{110}Sn

M. THOENNESSEN, E. RAMAKRISHNAN, J.R. BEENE, F.E. BERTRAND, M.L. HALBERT, D.J. HOREN, P.E. MUELLER, and R.L. VARNER

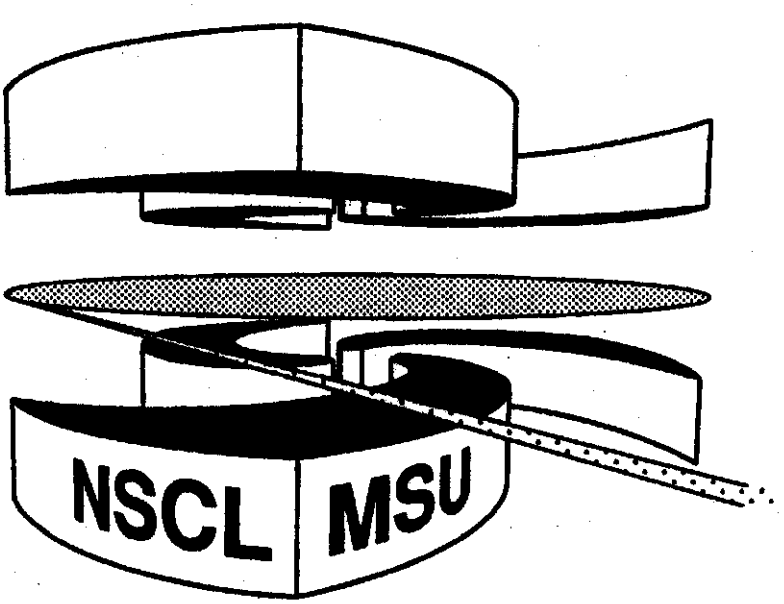

MSUCL-967

MARCH 1995

Dynamical Effects in Fusion Reactions Forming ^{110}Sn

M. Thoennessen and E. Ramakrishnan
National Cyclotron Laboratory and Department of Physics & Astronomy
Michigan State University, East Lansing, Michigan 48824

J. R. Beene, F. E. Bertrand, M. L. Halbert, D. J. Horen, P. E. Mueller, and R. L. Varner
Oak Ridge National Laboratory, Oak Ridge, Tennessee 37831
(March 2, 1995)

High energy γ-ray spectra were measured following the reactions ^{18}O + ^{92}Mo and ^{50}Ti + ^{60}Ni forming the compound nucleus ^{110}Sn at the same excitation energy of 56 MeV. The angular momentum gated γ-ray spectra from both reactions can be described by standard statistical model calculations. The influence of particle and γ-ray decay during the formation time is found to be small in both reactions. This result is consistent with predictions from dissipative dynamics calculations.

PACS 25.70.Gh,24.30Cz

I. INTRODUCTION

It has been known for a long time that dissipation influences heavy-ion reactions. One example of a process in which dissipation plays a role is mass transfer in deep-inelastic collisions; a second example is the hindrance of fusion in certain very symmetric reactions first explained within the framework of the dissipative dynamical model by Swiatecki and coworkers [1–3]. However, another effect that involves nearly symmetric reactions is still not fully understood. Neutron multiplicity measurements showed that the decay of certain fused systems depend on how they were formed [4,5] in apparent disagreement with Bohr's independence hypothesis. Subsequently, the effect was also observed in evaporation residue [6] and fission measurements [7]. Among other explanations it has been suggested that the discrepancies in the more symmetric system were due to differences in the formation times. However, these measurements are still controversial and the results of the neutron multiplicity measurements were not confirmed in recent work [8,9].

A suitable probe for investigating effects in the early stages of the compound nucleus formation and decay are high energy γ rays emitted from the giant dipole resonance (GDR) built on highly excited states. The γ rays are predominantly emitted during the first steps of the compound nucleus decay and the distribution of GDR strength is sensitive to the shape of the emitting system. The γ-ray decay of the GDR following fusion reactions is well understood [10,11] and has been employed in other contexts to study dynamical effects. It has been employed in the study of dissipation effects in fission reactions [12] which also were first observed in neutron multiplicity measurements [13] and subsequently extensively studied with γ rays from the GDR [14].

Recently the dynamical effects in the fusion evaporation reactions in nearly symmetric heavy-ion collisions were also observed with the GDR γ rays. The observations were interpreted in terms of long formation times during which particle and γ-ray emission was possible and subsequently influenced the decay of the compound nucleus [15]. This effect could be qualitatively explained by a model incorporating dissipation.

The model predicts that the long fusion time should depend not only on the mass asymmetry of the reactants, but also on the effective fissility of the combined system. In order to test the latter prediction we performed an experiment similar to that reported in Ref. [15] using two reactions with different mass asymmetries leading to a compound system with a smaller effective fissility.

We used the reactions ^{18}O + ^{92}Mo and ^{50}Ti + ^{60}Ni forming the compound nucleus ^{110}Sn at 56 MeV to study the possible differences of the dissipative effects in asymmetric and nearly symmetric reactions in a lighter mass region than in Ref. [15]. According to the dissipative dynamics models the formation time should be small. We chose the compound nucleus ^{110}Sn because the GDR strength function has been measured over a wide range of excitation energies [16–19]. In addition ^{110}Sn is on the average spherical even at hiih temperatures [17,20] and should exhibit a GDR strength function with a single Lorentzian component. This should increase the sensitivity to nonspherical shapes arising from reaction dynamieel effects.

II. EXPERIMENTAL PROCEDURE

The experiments were performed using 72 MeV ^{18}O and 163 MeV ^{50}Ti beams from the Holifield Heavy Ion Research Facility (HHIRF)at Oak Ridge National Laboratory (ORNL). Self-supporting isotopically enriched ^{92}Mo (1.83 mg/cm^2) and ^{60}Ni (656 μg/cm^2) targets were placed inside the Spin Spectrometer [21]. The beam energies were chosen so that the two reactions would form the compound nucleus ^{110}Sn at the same excitation energy of 56 MeV. The target thicknesses were chosen to give similar spread of excitation energy. High-energy γ rays (4 - 25 MeV) were detected with five close-packed clusters of 19 hexagonal BaF_2 scintillation detectors each. Four of the clusters consisted of detectors belonging to the ORNL BaF_2 array, with individual detectors 20 cm long and having a hexagonal cross section with an inscribed diameter of 6.5 cm. The fifth cluster of 19 detectors from Michigan State University (MSU) had slightly different dimensions (25 cm long, 6 cm inscribed diameter). Two clusters were positioned at 21°, two clusters at 63°, and one cluster at 117°. The clusters at backward and forward angles were placed at 57 cm and 77 cm from the target, respectively. At these positions NaI(Tl) detectors were removed from the Spin Spectrometer to allow the BaF_2 arrays unobstructed views of the target.

The HHIRF 25MV tandem accelerator delivered a dc beam. Neutron – γ-ray separation was achieved by timing the BaF_2 array against an average time deduced from at least three low-energy γ-ray transitions detected inside the Spin Spectrometer [22,23]. This method does not distinguish beam-induced events from cosmic ray muons passing through both the Spin Spectrometer and one of the BaF_2 clusters. The cosmic-ray events could be clearly identified in a two-dimensional plot of the total γ-ray energy deposited in the BaF_2 and the NaI(Tl) detectors versus the multiplicity in the Spin Spectrometer; they occur at very large energies and relatively small multiplicities, and most of them were eliminated in the off-line analysis.

The γ-ray detectors were energy calibrated using sources of ^{88}Y (0.898 MeV and 1.836 MeV) and ^{228}Th (2.615 MeV), inelastic proton scattering by ^{12}C (4.439 MeV and 15.11 MeV) and with the broad peak corresponding to energy deposition by cosmic ray muons passing through the detectors configured in a horizontal position for which the most probable energy-loss is 40.3 MeV and 37.9 MeV for the ORNL and MSU detectors, respectively. The temperature within the arrays was continuously monitored and included in the data stream. The temperature fluctuations during the run were so small that no corrections of the energy calibrations were necessary.

The γ-ray spectra were generated off line by summing the γ-ray energy within each cluster, after gain matching and neutron separation, in order to improve the detector response. The total γ-ray spectrum is then the sum of the five individual cluster spectra. Small contributions from the remaining cosmic-ray background events were removed by subtraction of spectra measured under the same conditions as the real experiment but with no beam; these spectra were normalized beyond energies of 24 MeV.

It is well established that an approximately linear relation exists between the internal angular momentum of a compound nucleus and the total number of γ rays emitted in its decay. Thus the γ-ray multiplicity serves as a good experimental measure of angular momentum. In collisions at energies close to the coulomb barrier, such as the ones studied here, inelastic and deep inelastic processes transfer only small amounts of angular momentum to the reaction products. Consequently the Spin Spectrometer, used as a γ-ray multiplicity filter, provides very good discrimination against these low angular momentum processes.

III. STATISTICAL MODEL ANALYSIS

Although the experimental conditions were chosen to populate the ^{110}Sn compound nucleus at the same excitation energy it was not possible to simultaneously match the angular momentum distribution produced in the two reactions. Thus it is necessary to select similar angular momentum populations before the final γ-ray spectra can be directly compared. The Spin Spectrometer measures the γ-ray fold i.e. the number of NaI crystals triggered by γ-rays in each event and its design is such that the γ-ray fold is closely related to the γ-ray multiplicity [21].

In order to determine the effect of a γ-ray fold gate on the angular momentum selection of the compound nucleus, it is necessary to consider the relationship between angular momentum and γ-ray multiplicity in the decay of ^{110}Sn and the response of the Spin Spectrometer. This was done using the statistical model code EVAP [24] to simulate the decay of the compound system and a code based on the GEANT3 [25] package to simulate the response of the Spin Spectrometer. In this way a transfer matrix from γ-ray fold to angular momentum was constructed. The region of angular momentum selected by the applied fold gate is inferred from this simulated transformation and on the initial distribution of angular-momentum states populated by the reaction. No experimental data on this distribution exists for either reaction. The intial angular momentum distributions were therefore calculated with the sum-rule model [26]. This model reproduced the measured fusion cross sections for ^{18}O + ^{92}Mo at slightly lower beam energies [27]. Total fold distributions were calculated using the simulated angular momentum to fold response and the calculated angular momentum distributions. The resulting fold distributions (o) are compared to experimental data (•) in Figure 1 for the two reactions ^{18}O + ^{92}Mo and ^{50}Ti + ^{60}Ni. The same method was applied in the previous ex-

periment [15] where the corresponding angular momentum distributions were measured [22].

The effect of the fold gate (accepted fold gates = 5 to 10) can then be obtained from the simulated responses and the calculated angular momentum distribution. The resulting fold-selected angular momentum distributions are shown in Figure 2 for the ^{18}O (■) and ^{50}Ti (◇) induced reactions. In both reactions the fold gate selects predominantly angular momenta between 15-30 $\hbar$ with some small contributions of higher angular momenta in the ^{50}Ti + ^{60}Ni reaction.

The angular momentum distributions calculated in this way were used as the initial distributions for the statistical model calculations using CASCADE [28]. The final extracted γ-ray spectra were folded with the response function of the BaF_2 arrays as calculated with GEANT3.

Figure 3 shows the γ-ray spectra for the reaction ^{18}O + ^{92}Mo and ^{50}Ti + ^{60}Ni together with the results of the CASCADE calculations. The two γ-ray spectra are essentially identical. Both could be fitted with the same set of statistical model parameters. A level density parameter of A/10 was used and an overall strength of 90±10 % of the energy-weighted sum rule was obtained. As expected both spectra could be fitted with a single Lorentzian strength function with E_{GDR} = 14.7±0.2 MeV and Γ_{GDR} = 7.3±0.5 MeV, in good agreement with previously measured data [16,17]. Thus, no signs of significant entrance channel effects are evident in this pair of reactions.

In order to display any possible differences more clearly, Figure 4 shows the same data as Figure 3 on a linear scale. In this figure the data and the fits from both reactions were divided by the same calculation obtained using a constant strength function. It is apparent that the γ-ray spectra from the two reactions show no statistically significant differences. In addition Figure 4 displays the quality of the fits. The small difference between the two reactions arises because of differences in the angular momentum distribution at large angular momenta selected by the gate on the γ-ray fold. This figure, therefore, serves as an illustration of the size of effects expected due to imperfectly matched angular momentum distributions.

IV. DISSIPATIVE DYNAMICS CALCULATIONS

The existence of entrance channel effects observed in the A ~ 160 mass region could be qualitatively understood with long formation times leading to the compound system for the more symmetric reactions [15]. These long formation times can be explained by including dissipation in the heavy-ion collision calculation [2]. This model can be used to provide guidance as to when dissipative dynamical effects might be significant for fusion reactions. Swiatecki [2] has provided an illuminating discussion of important effects in this picture. This discussion isolates two important parameters in the model. The relative fissility is defined as

$$X_0 = Z^2e^2/(16\pi\gamma R^3)$$

where γ is the liquid drop surface-energy coefficient. The entrance channel asymmetry of the reaction is defined as

$$\Delta = (R_1 - R_2)/(R_1 + R_2)$$

where R, R_1, and R_2 are the radii of the compound system, the projectile and the target, respectively. In addition, the effective fissility is defined as

$$x = X_0 \cdot (1 - \Delta^2)/(1 + 3\Delta).$$

Figure 5 shows the asymmetry as a function of relative fissility for the reactions ^{18}O + ^{92}Mo and ^{50}Ti + ^{60}Ni as well as the previously measured reactions ^{16}O + ^{148}Sm and ^{64}Ni + ^{100}Mo. In addition a line indicating the relative fissility x = 0.57 is drawn. This value of x defines the critical fissility x_c: For systems with $x < x_c$ dissipative effects are expected to be small and a system with kinetic energy larger than the static interaction barrier fuses and equilibrates rapidly, whereas for $x > x_c$ dissipative effects impede fusion and the dynamical evolution toward an equilibrated system should be slower. Effects like the "extra push" and deep inelastic collisions become significant in this region for small impact parameters and just above the interaction barrier. Swiatecki derived x_c = 0.57 on theoretical grounds [2]; experiments investigating the "extra push" effect indicated $x_c \sim 0.7$ [29]. Figure 5 shows x_c for angular momentum of $l = 0$. The critical fissility is smaller for larger angular momenta. The figure should serve only as a qualitative guidance that to the left and above the $x = x_c$ line dissipative dynamical effects are expected to be small. Of the four reactions shown, only ^{64}Ni + ^{100}Mo is located in the region where dissipation plays a significant role. Even though the ^{50}Ti + ^{60}Ni reaction is more symmetric than ^{64}Ni + ^{100}Mo, the low fissility of this system pushes it quite far outside the dissipative region.

Feldmeier incorporated Swiatecki's ideas of macroscopic dissipative dynamics into his particle exchange model code HICOL [30,31]. We have used this code to calculate the time evolution of the collisions. Figure 6 shows the shape evolution of the reactions ^{18}O + ^{92}Mo, ^{50}Ti + ^{60}Ni, ^{16}O + ^{148}Sm, and ^{64}Ni + ^{100}Mo at an angular momentum of 25 $\hbar$ corresponding to impact parameters of 3.9 fm, 2.6 fm, 3.3 fm and 1.5 fm respectively. The more symmetric reactions evolve more slowly than the asymmetric reactions. Even though the impact parameters are smaller for the symmetric reactions it can be seen that they go through stages of much larger deformation. The ^{64}Ni + ^{100}Mo reaction takes much longer than

the other three reactions (about a factor of 5) to reach full shape equilibration that might be identified with a compound nucleus, as predicted qualitatively by Figure 6.

Figure 7 shows the time evolution of two characteristics of the reactions as described by HICOL at an angular momentum of 25 $\hbar$ as in Figure 6. The upper panel shows the time dependence of the effective excitation energy of the approaching systems as they reach a thermal equilibrium. The shape equilibration is illustrated in the lower panel, parameterized in terms of the distance between the centers of the two colliding ions. The figure indicates that the time scales characterizing the shape equilibration of the $^{18}O + {}^{92}Mo$ and $^{50}Ti + {}^{60}Ni$ reactions ($\sim 20 \times 10^{-22}$s) differ by a factor of almost two.

These time scales should be compared to the particle evaporation times of the compound nuclei in order to see whether evaporation is significant during the formation process. Although neutron evaporation is the strongest channel in the decay of ^{110}Sn, proton and α-evaporation cannot be neglected. At an excitation energy of 56 MeV the angular momentum averaged decay widths for neutron, proton, and α emissions are 61 keV, 26 keV, and 16 keV, respectively. The total lifetime for first decay step is then on average $\sim 64 \times 10^{-22}$s. These lifetimes are comparable to the formation times of $\sim 20 - 40 \times 10^{-22}$s for the $^{18}O + {}^{92}Mo$ and $^{50}Ti + {}^{60}Ni$ systems. Thus the possible particle and γ-ray decay during this formation was incorporated in the evaporation code to investigate its influence on the decay of the compound nucleus.

V. STATISTICAL DECAY DURING COMPOUND NUCLEUS FORMATION

The deviations of the γ-ray spectra from results of standard statistical model calculation observed in the $^{64}Ni + {}^{100}Mo$ reaction have been estimated by modifying and expanding the standard statistical code CASCADE to include particle and γ-ray emission during the formation period of the compound nucleus [15]. In a first approach the total decay was divided into two parts: (i) decay during formation and (ii) compound nucleus decay. Instead of following the evolution of the relevant parameters as a function of time during the formation, only the average values were estimated and the time for the possible decay was limited to the formation time. It should be noted that this approach can only be taken as a qualitative estimate because the statistical model is being applied to a clearly non-equilibrated system.

The modifications to CASCADE were incorporated into the version of the code which was used to calculate the pre-scission decay of fission reactions [32,33]. The present situation is quite similar. The decay during the formation can be described essentially in the same way as the saddle-to-scission decay during fission [33]. Both processes are limited to a finite time during which the thermal energy and the shape of the composite system changes. At the end of the formation period the resulting population distribution is spread over a range of excitation energies, angular momenta, and different nuclei according to the particle and γ-ray decay during the formation. These distributions serve as the input population distributions for the compound nucleus decay (of several different nuclei). The code was tested by setting the formation time to zero; this resulted, as it should have, in spectra identical to those predicted by the unmodified CASCADE.

The input parameters for the formation period calculations were based upon the results of the HICOL calculations. The mean excitation energy was estimated to be 30 MeV and 35 MeV for $^{18}O + {}^{92}Mo$ and $^{50}Ti + {}^{60}Ni$, respectively (see Figure 7). The average deformation, and thus the splitting of the GDR, was derived from the separation s of the centers of the collinding ions as defined in Ref. [30]. In a crude approximation the shape was assumed to be ellipsoidal and the long axis r_l was calculated with the relation $r_l = (s + r_{proj} + r_{targ})/2$ where s was estimated from Figure 7. The short axis r_s of the ellipsoid was then be derived with the assumption of volume conservation. The radii of the principal axes r_l and r_s where related to the corresponding GDR energies E_l and E_s by assuming that the GDR energy is inversely proportional to the radius. The radius of the spherical ^{110}Sn was taken to be 5.8 fm and the resonance energy $E_0 = 14.5$ MeV was based on the analysis in Section III. The GDR widths Γ_l and Γ_s were calculated using the relationship [34,35]

$$\Gamma_i = (E_i/E_0)^{1/1.6}\Gamma_0$$

where $i = l, s$ correspond to vibrations along the long and short axes, r_l and r_s, respectively. The width for spherical ^{110}Sn at $E^* = 30$ MeV was taken to be $\Gamma_0 = 5.5$ MeV [17]. The estimated radii and calculated GDR parameters which were used in the statistical model are listed in Table I for $^{18}O + {}^{92}Mo$ and $^{50}Ti + {}^{60}Ni$.

The level density parameter during the formation period was chosen to be A/15 which was previously necessary to fit the $^{64}Ni + {}^{100}Mo$ data [15] and was justified with rather small level densities for superdeformed shapes [36]. The formation times, based on the HICOL results, were $\tau_f = 20 \cdot 10^{-22}s$ and $\tau_f = 40 \cdot 10^{-22}s$ for $^{18}O + {}^{92}Mo$ and $^{50}Ti + {}^{60}Ni$, respectively. All the other parameters were identical to those used in the standard statistical model calculations described previously. The second stage of the code, the decay of the equilibrated compound nuclei populated after the end of the formation period, is calculated with the same parameters used in the standard statistical model calculations.

Figure 8 shows the results of these calculations for $^{18}O + {}^{92}Mo$ and $^{50}Ti + {}^{60}Ni$. The total γ-ray spectrum is the sum of two contributions; γ rays emitted during the formation period and γ rays originating from the compound nuclei. The large deformation and the resulting

large splitting of the GDR during formation is reflected in the shape of the dashed contribution. It is obvious that this contribution to the total γ-ray spectra is not significant. It is somewhat larger for the ^{50}Ti + ^{60}Ni reaction as a result of the longer formation time. Calculations using a level density of A/13 reduced the contribution of the formation period by $\sim$ 40 %.

The particle and γ-ray decay during formation also influences the subsequent γ-ray spectra of the compound nuclei as can be seen in Figure 9. In this figure the data and the calculations are again displayed on a linear scale as in Figure 4 by dividing the data and the calculations by another calculation with a constant energy-independent strength function. The lines of the individual contributions are the same as in Figure 8.

The compound nucleus contribution is slightly lower due to the reduced average excitation energy of the compound systems following the decay during the formation. The (small) contribution from the latter added together with the compound contribution give a good description of the data. The reduction of the average excitation energy of the compound system can be calculated from Table II. The table lists the relative probability for the population and average excitation energy of the different compound nuclei resulting from decay during formation. The mean initial excitation energy averaged over these compound nuclei is 51.6 MeV and 48.9 MeV for the ^{18}O + ^{92}Mo and ^{50}Ti + ^{60}Ni reactions, respectively. These values are to be compared to the initial compound nucleus excitation energy of 56 MeV for the standard statistical model calculation performed as described in Section III. The branching ratio for high-energy γ-ray emission is a strong function of the excitation energy and thus the high energy γ-ray contribution of the compound nuclei is slightly reduced with respect to the standard statistical model calculation. However, the sum of both contributions gives a very good fit to the data.

Both reactions can be described with the standard statistical model as well as with the modified version which includes decay during the formation period. In ^{110}Sn the formation-stage contributions are small so that the overall spectral shape is not changed significantly.

In addition to the γ-ray spectra the statistical model calculations also predict the particle multiplicities. These yielded the first evidence for entrance channel effects [4,5]. Table III lists the total neutron, proton and α multiplicities (M_{tot}) for the two reactions, as well as the individual contributions from decay during formation (M_F) and the following compound nuclear decay (M_{CN}). The formation-stage contribution is $<$ 10% and $<$ 15% for the ^{18}O and ^{50}Ti induced reactions, respectively. The larger values for ^{50}Ti + ^{60}Ni are due to the larger formation time. The sum of both contributions is exactly equal to the multiplicities calculated with the standard statistical model. This is consistent with the conclusion from the γ-ray spectra; the formation period does not contribute significantly and the data can be completely described by the standard statistical model. The slightly wider angular momentum distribution in the ^{50}Ti + ^{60}Ni reaction, which reduces the effective mean excitation energy because of the larger rotational energy, results in a reduced overall particle multiplicity in the ^{50}Ti + ^{60}Ni reaction. This shows that the neutron multiplicities are extremely sensitive to the fold gate, whereas this gate is not as crucial for the γ-ray spectra.

Even in the reaction ^{64}Ni + ^{100}Mo where significant differences in the γ-ray spectra due to decay during the formation period were observed, the total particle multiplicities from the formation and the compound decay are equal to the total multiplicities calculated with the standard model. This effect is currently being investigated in the ^{164}Yb system in detail [37].

VI. DISCUSSION AND CONCLUSION

The small contribution of the formation period to the total γ-ray spectra in the two fusion reactions yielding ^{110}Sn studied here is in agreement with the dynamical calculations performed with HICOL. This is in contrast to the observations in the heavier (A $\sim$ 164) system where the γ-ray spectra in the reaction ^{64}Ni + ^{100}Mo could only be described by assuming formation times which were a factor of two larger than predicted by HICOL. Also, within the present simplified model it was essential to choose a rather low level-density parameter (A/15) for the formation period [15]; larger level-density parameters increase the discrepancies, but in the A $\sim$ 110 system the data can be described equally well with a larger level-density parameter (A/13). An increase of the formation times in the reaction ^{50}Ti + ^{60}Ni does not seem to describe the data, as shown in the top of Fig. 10. The calculations were performed with the parameters of the fits shown in Fig. 9 except that the formation time was increased to 80×10^{-21}s. However, with a small adjustment of the compound nucleus GDR parameters it is possible to achieve very good fits to the data. The bottom part of Fig. 10 shows a calculation with a formation time of 80×10^{-21}s, but with a slightly lower resonance energy, E_{GDR} = 14 MeV, and a smaller width, Γ_{GDR} = 6.0 MeV. The assumed larger formation time reduces the effective excitation energy even further, resulting in a smaller resonance width which is a function of the excitation energy.

The current system with A $\sim$ 110 is, therefore, not sensitive to any deviations within the dissipation model. The origin of the large formation time in the ^{64}Ni + ^{100}Mo reaction should be studied in this mass region.

One possible explanation for the longer time could be the simplification of using the times calculated for an angular momentum of 25 $\hbar$ in the present calculations. Fig. 11 shows that the formation time can be a strong function of the angular momentum [38]. The formation time for the ^{50}Ti + ^{60}Ni reaction increases almost linearly from $30 \cdot 10^{-22}$s to $50 \cdot 10^{-22}$s for angular momentum be-

tween 0 $\hbar$ and 30 $\hbar$. However, the reaction ^{64}Ni + ^{100}Mo shows a dramatic increase of the formation time around 30 $\hbar$. The semiclassical code HICOL does not predict fusion to occur for this system for angular momenta larger than 30 $\hbar$, but it is well known that quantum mechanical coupled-channel and/or particle-transfer effects enhance the fusion cross section in certain cases allowing fusion to occur at much larger angular momenta [39]. The angular momentum distribution for ^{64}Ni + ^{100}Mo fusion has been measured and extends well above 40 $\hbar$ [22]. In this reaction the fold gate applied to the γ-ray spectra has $\sim$ 20% contribution from angular momenta $>$ 30 $\hbar$ [15]. This might account for the discrepancy between the measured and calculated formation times in this system. It would be extremely interesting to calculate the formation times at higher angular momenta.

The dependence of the formation time on the excitation energy ought to be studied. At larger excitation energies, the influence of decay during formation must vanish. This can be inferred from existing data in the rare earth region where measurements of high energy γ rays following the fusion of near-symmetric systems around 80-90 MeV excitation energy can be fully described by the standard statistical model [40,41]. This indicates that, as in the present system, the formation effects do not play a significant role.

The detailed interpretation of these analyses should be taken with care because the model of statistical decay during formation, describing this stage within one single step, is rather crude. A more elaborate description of the formation period which follows the shape and excitation energy evolution as a function of time is being developed. Initial calculations with this model seem to confirm the need for a longer formation time for the reaction ^{64}Ni + ^{100}Mo [37].

It should be mentioned that the observed deviations from the standard statistical model in the ^{64}Ni + ^{100}Mo system do not violate Bohr's independence hypothesis since the compound nucleus is formed with different conditions due to the prior emission of particles and γ rays (see Tables II and III).

In summary, we have measured high energy γ-ray spectra following the fusion reactions ^{18}O + ^{92}Mo and ^{50}Ti + ^{60}Ni forming ^{110}Sn at 56 MeV excitation energy. Both reactions can be described by the standard statistical model. A model which includes the possibility of particle and γ-ray decay during formation of the compound nucleus also describes the data. The formation times of $20 \cdot 10^{-22}$s and $40 \cdot 10^{-22}$s extracted from a dissipative dynamical model for the reactions ^{18}O + ^{92}Mo and ^{50}Ti + ^{60}Ni, respectively, are too short to yield significant contributions from the formation stage to the total γ-ray spectrum. Thus the data are consistent with the dissipative description of the heavy-ion fusion reactions.

ACKNOWLEDGMENTS

This work was partially supported by the U.S. National Science Foundation under Grant No. PHY-92-14992. Oak Ridge National Laboratory is managed by Martin Marietta Energy Systems, Inc. under contract DE-AC05-84OR21400 with the U.S. Department of Energy.

[1] J. Blocki, J. Randrup, W. J. Swiatecki, and C. F. Tsang, Ann. Phys. (N.Y.) **105**, (1977).
[2] W. J. Swiatecki, Physica Scripta **24**, 113 (1981).
[3] S. Bjørnholm and W. J. Swiatecki, Nucl. Phys. **A391**, 471 (1982).
[4] W. Kühn, P. Chowdhury, R. V. F. Janssens, T. L. Khoo, F. Haas, J. Kasagi, and R. M. Ronningen, Phys. Rev. Lett. **51**, 1858 (1983).
[5] R. V. F. Janssens, R. Holzmann, W. Henning, T. L. Khoo, K. T. Lesko, G. S. F. Stephans, D. C. Radford, A. M. van den Berg, W. Kühn, and R. M. Ronningen, Phys. Lett. **181B**, 16 (1986).
[6] A. Ruckelshausen *et al.*, Phys. Rev. Lett. **56**, 2356 (1986); Phys. Rev. Lett. **58**, 1584 (1987).
[7] F. L. H. Wolfs, R. V. F. Janssens, R. Holzmann, T. L. Khoo, W. C. Ma, and S. J. Sanders, Phys. Rev. **C39**, 865 (1989).
[8] B. Fornal *et al.*, Phys. Rev. **C42**, 1472 (1990).
[9] J. L. Barreto *et al.*, Phys. Rev. **C48**, 2881 (1993).
[10] K. A. Snover, Ann. Rev. Nucl. Part. Sci. **36**, 545 (1986).
[11] J. J. Gaardhøje, Ann. Rev. Nucl. Part. Sci. **42** (1992).
[12] M. Thoennessen, D. R. Chakrabarty, M. G. Herman, R. Butsch, and P.Paul, Phys. Rev. Lett. **59**, 2860 (1987).
[13] D. Hilscher, H. Rossner, Ann. Phys. Fr. **17**, 471 (1992).
[14] P. Paul and M. Thoennessen, Ann. Rev. Nucl. Part. Sci. **44**, in press (1994).
[15] M. Thoennessen, J. R. Beene, F. E. Bertrand, C. Baktash, M. L .Halbert, D. J. Horen, D. G. Sarantites, W. Spang, and D. W. Stracener, Phys. Rev. Lett. **70**, 4055 (1993).
[16] J. J. Gaardhøje, C. Ellegaard, B. Herskind, R. M. Diamond, M. A. Delaplanque, G. Dines, A. O. Macchiavelli, and F. S. Stephens, Phys. Rev. Lett. **56**, 1783 (1986).
[17] D. R. Chakrabarty, S. Sen, M. Thoennessen, N. Alamanos, P. Paul, R. Schicker, J. Stachel, and J. J. Gaardhøje, Phys. Rev. **C36**, 1886 (1987).
[18] A. Bracco *et al.*, Phys. Rev. Lett. **62**, 2080 (1989).
[19] F. Camera, A. Bracco, B. Million, M. Pignanelli, J. J. Gaardhøje, A. Maj, and A. Atac, Phys. Lett. **293B**, 18 (1992).
[20] Z. Majka *et al.* Phys. Rev. Lett. **58**, 322 (1987),
[21] M. Jääskeläinen, D. G. Sarantites, R. Woodward, F. A. Dilmanian, J. T. Hood, R. Jääskeläinen, D. C. Hensley, M. L. Halbert, and J. H. Barker, Nucl. Instr. and Meth. **A204**, 385 (1983).

[22] M. L. Halbert, J. R. Beene, D. C. Hensley, K. Honkanen, T. M. Semkow, V. Abenante, D. G. Sarantites, and Z. Li, Phys. Rev C **40** 2558 (1989).
[23] M. Thoennessen *et al.*, Inst. Phys. Conf. Ser. **109**, 135 (1991).
[24] N. G. Nicolis, J. R. Beene, Code EVAP.
[25] R. Brun, F. Bruyant, M. Maire, A. C. McPherson, and P. Zanarini, GEANT3 Users Guide, Data Handling Division DD/EE/84-1, CERN 1986.
[26] J. Wilczynski, K. Siwek-Wilczynska, J. van Driel, S. Gonggrijp, D. C. J. M. Hageman, R. V. F. Janssens, J. Lukasiak, and R. A. Siemssen, Phys. Rev. Lett. **45**, 606 (1980).
[27] M. Benjelloun, W. Galster, and J. Vervier, Nucl. Phys. **A560**, 715 (1993).
[28] F. Pühlhofer, Nucl. Phys. **A260**, 276 (1977).
[29] J. Blocki, H. Feldmeier, and W. J. Swiatecki, Nucl. Phys. **A459**, 145 (1986).
[30] H. Feldmeier, Program HICOL (1986).
[31] H. Feldmeier, Rep. Prog. Phys. **50**, 915 (1987).
[32] R. Butsch, M. Thoennessen, D. R. Chakrabarty, M. G. Herman, and P. Paul, Phys. Rev. **C41**, 1530 (1990).
[33] R. Butsch, D. J. Hofman, C. P. Montoya, P. Paul, and M. Thoennessen, Phys. Rev. C **44**, 1515 (1991).
[34] Y. Alhassid and B. Bush, Nucl. Phys. **A509**, 461, (1990).
[35] Y. Alhassid and B. Bush, Nucl. Phys. **A531**, 1, (1991).
[36] K. Schiffer and B. Herskind, Nucl. Phys. **A520**, 521c, (1990).
[37] J. R. Beene, M. L. Halbert, and M. Thoennessen, to be published.
[38] M. Thoennessen and J. R. Beene, Proc. Symp. "Reflections and Directions in Low Energy Heavy Ion Physics", Edited by J. H. Hamilton, H. K. Carter, L. L. Riedinger, and R. L. Robinson, p.149, World Scientific (Singapore, 1993).
[39] M. Beckerman, Phys. Rep. **B129**, 145 (1985).
[40] A. M. Bruce, J. J. Gaardhøje, B. Herskind, R. Chapman, J. C. Lisle, F. Khazaie, J. N. Mo, and P. J. Twin, Phys. Lett. **B215**, 237, (1988).
[41] A. Stolk, M. N. Harakeh, W. H. A. Hesselink, H. J. Hofmann, R. F. Noorman, J. P. S. van Schagen, Z. Sujkowski, H. Verheul, M. J. A. de Voigt, and D. J. P. Witte, Phys. Rev. **C40**, R2454, (1989).

TABLE I. Average calculated shape and deduced GDR parameters for the decay calculation during the formation stage

	$^{18}O + ^{92}Mo$	$^{50}Ti + ^{60}Ni$
$s(fm)$	7	8
$r_l(fm)$	7.8	8.6
$r_s(fm)$	4.7	4.5
E_l (MeV)	10.7	9.7
E_s (MeV)	16.9	17.7
Γ_l (MeV)	4.5	4.3
Γ_s (MeV)	6.1	6.2

TABLE II. Compound nuclei (CN) populated following the decay during formation. The corresponding decay channel as well as the relative population (%) and average initial excitation energies E^* (MeV) are given for each compound nucleus for the two reactions

		$^{18}O + ^{92}Mo$		$^{50}Ti + ^{60}Ni$	
CN	Decay mode	Population (%)	E^* (MeV)	Population (%)	E^* (MeV)
^{110}Sn	0n	73.4	56.0	57.5	56.0
^{109}Sn	1n	15.1	40.6	23.1	40.6
^{109}In	1p	6.7	39.6	10.3	39.5
^{108}Sn	2n	0.28	30.0	0.93	29.9
^{108}In	1n1p	0.25	27.3	0.83	27.1
^{106}Cd	1α	4.2	37.8	7.0	37.7
^{105}Cd	1n1α	0.07	25.9	0.26	25.8
^{105}Ag	1p1α	0.01	24.5	0.04	24.5

TABLE III. Calculated neutron, proton, and α multiplicity for the formation stage M_F, the compound nuclear stage M_{CN}, and the sum M_{tot}, which is identical to the multiplicities calculated with the standard statistical model.

	M_F	M_{CN}	M_{tot}
	$^{18}O + ^{92}Mo$		
n	0.16	1.76	1.92
p	0.07	0.89	0.96
α	0.04	0.45	0.49
	$^{50}Ti + ^{60}Ni$		
n	0.26	1.56	1.82
p	0.11	0.77	0.88
α	0.07	0.51	0.58

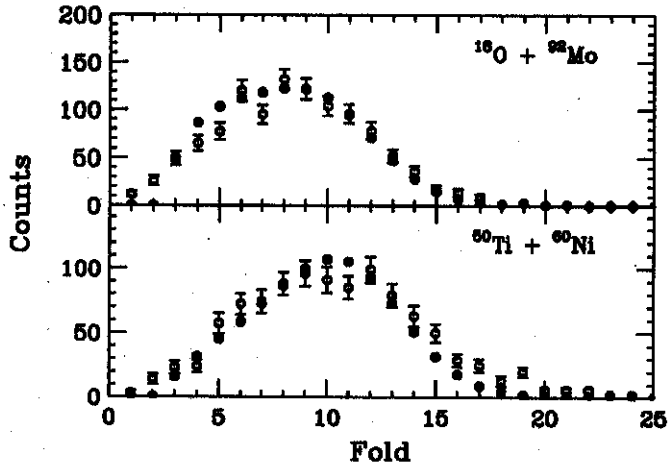

FIG. 1. Measured (•) and simulated (○) γ-ray fold distributions for the reactions $^{18}O + ^{92}Mo$ (top) and $^{50}Ti + ^{60}Ni$ (bottom).

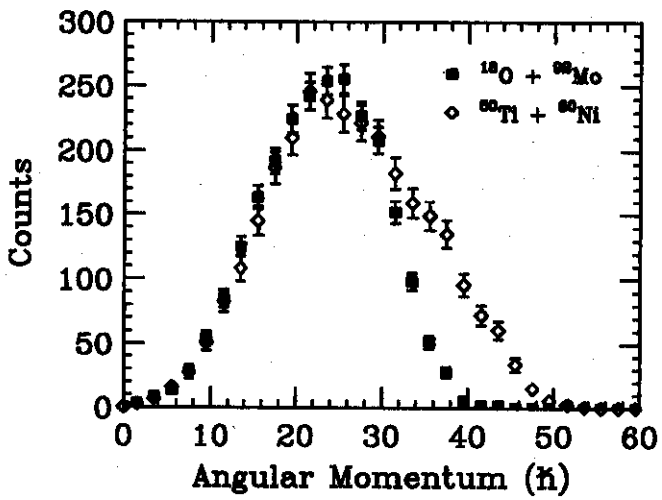

FIG. 2. Calculated spin distributions for the ^{18}O (■) and ^{50}Ti (◇) induced reactions corresponding to a fold gate of 5-10 applied to the γ-ray spectra.

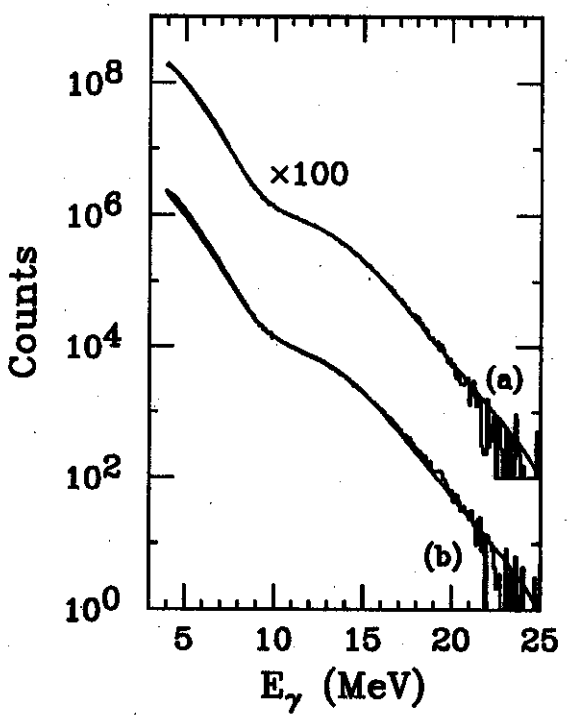

FIG. 3. Gamma-ray spectra of the compound nucleus decay of ^{110}Sn following the reactions $^{18}O + ^{92}Mo$ (a) and $^{50}Ti + ^{60}Ni$ (b). The solid lines are fits to the data (histograms) with standard statistical model calculations.

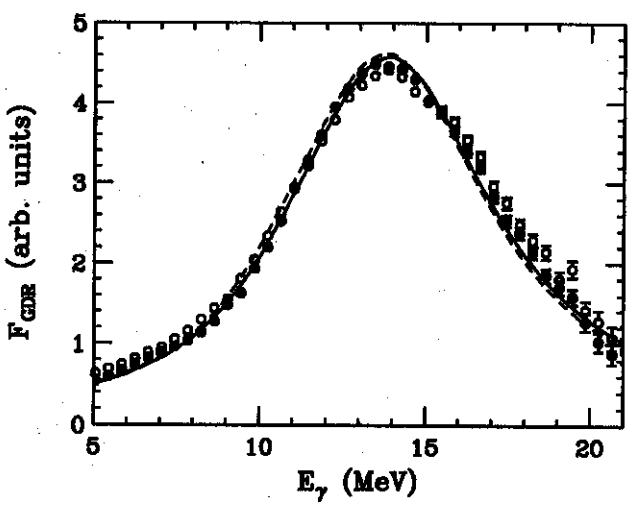

FIG. 4. Linearized plots of the γ-ray spectra for the ^{18}O (•, solid) and ^{50}Ti (○, dashed) induced reactions. The data as well as the calculations for both data sets were divided by the same constant strength function.

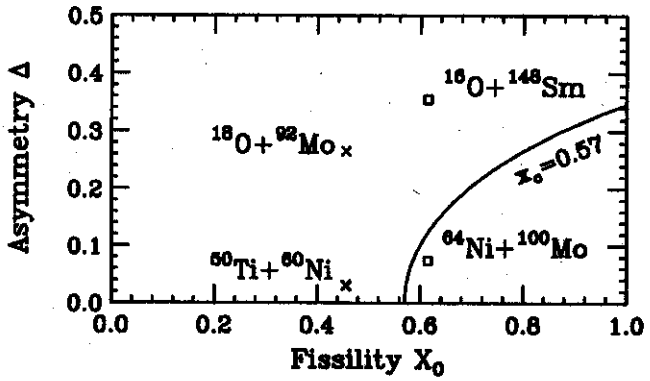

FIG. 5. Asymmetry Δ as a function of fissility X_0 for the compound nuclei ^{164}Yb (□) and ^{110}Sn (×). To the right of the line x = 0.57 deep-inelastic reactions are expected to appear for central collisions.

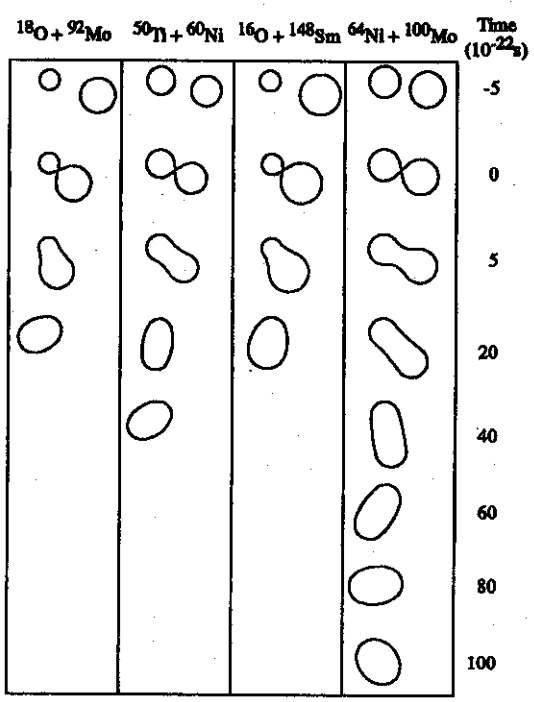

FIG. 6. Time evolution of the reactions ^{18}O + ^{92}Mo, ^{50}Ti + ^{60}Ni, ^{16}O + ^{148}Sm, and ^{64}Ni + ^{100}Mo for an angular momentum of 25 ħ.

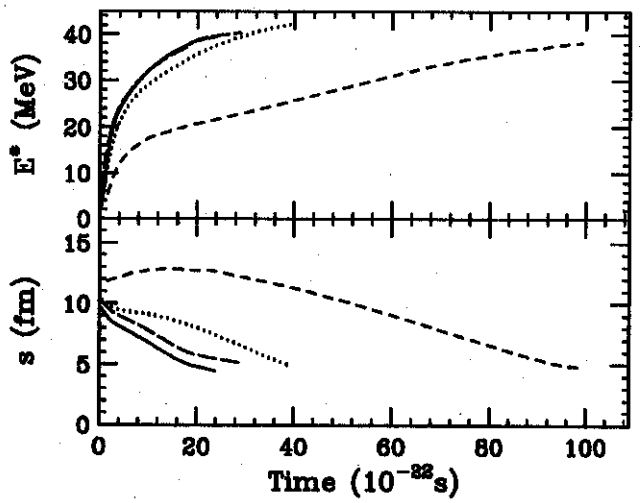

FIG. 7. Calculated evolution of the excitation energy (E^*) and the separation of the colliding nuclei (s) as a function of time for the reactions ^{18}O + ^{92}Mo (solid), ^{50}Ti + ^{60}Ni (dotted), ^{16}O + ^{148}Sm (long-dashed), and ^{64}Ni + ^{100}Mo (short-dashed) at an angular momentum of 25 ħ.

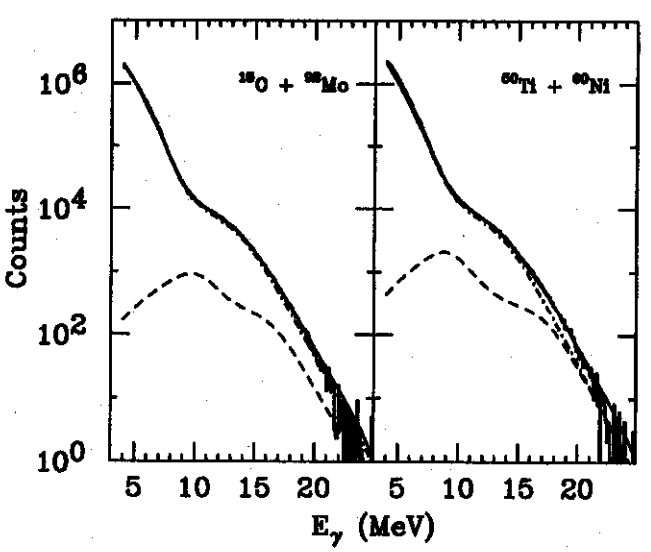

FIG. 8. Gamma-ray spectra following the reactions ^{18}O + ^{92}Mo (left) and ^{50}Ti + ^{60}Ni (right). The calculations (solid) are fits with the modified statistical model which are the sums of the contributions from the decay during the compound-nucleus formation (dashed) and the compound nucleus (dot-dashed) decay.

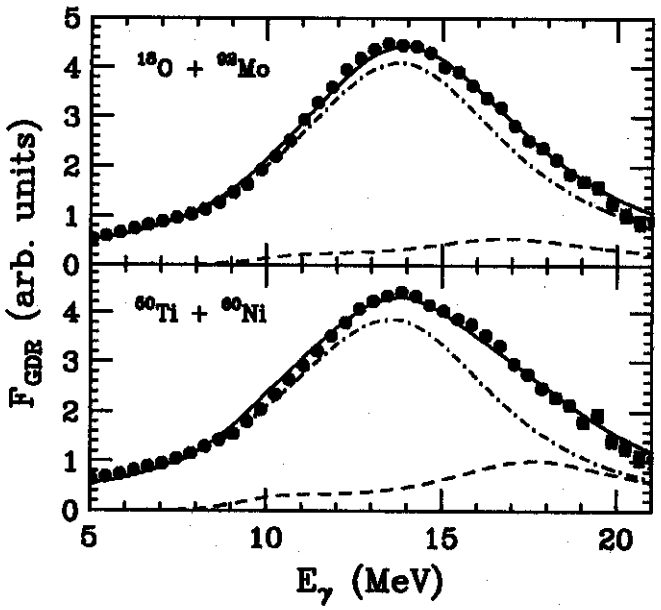

FIG. 9. Linearized plots of the γ-ray spectra for the ^{18}O (top) and ^{50}Ti (bottom) induced reactions as Figure 4. The solid lines are sums of the contributions from the formation (dashed) and the compound nucleus decay (dot-dashed).

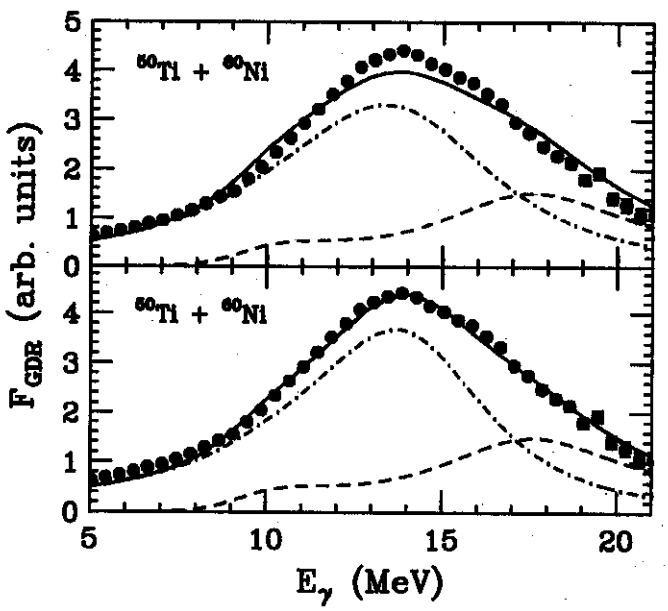

FIG. 10. Same as Figure 9 for the reaction ^{50}Ti. The calculations were performed with twice the formation times ($80 \cdot 10^{-22}$s). In the top part the same parameters were used as for the bottom part of Figure 9 whereas in the bottom part the GDR energy (E_{GDR} = 14.7 MeV) and width (Γ_{GDR} =6.0 MeV) of the compound nucleus contribution were adjusted to fit the data.

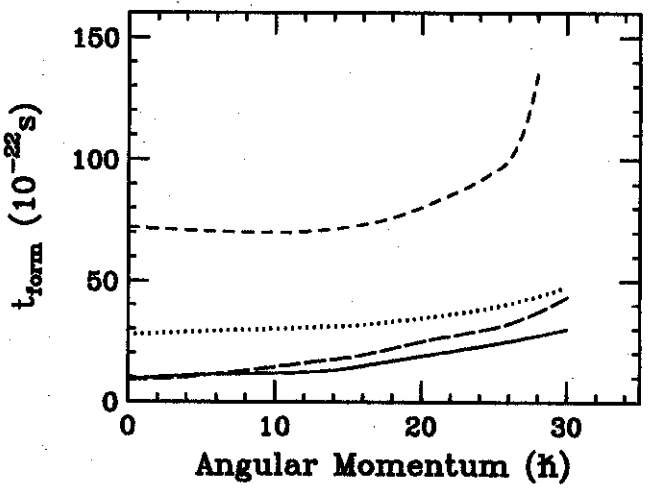

FIG. 11. Compound nucleus formation times as a function of angular momentum for the reactions $^{18}O + ^{92}Mo$ (solid), $^{50}Ti + ^{60}Ni$ (dots), $^{16}O + ^{148}Sm$ (long-dashed), and $^{64}Ni + ^{100}Mo$ (short-dashed).